DOI 10.24425/aee.2024.150896

Active flux based adaptive and non-adaptive observer for sensorless interior permanent magnet synchronous machine drive

Deepak Vyas ✉, Marcin Morawiec, Tadele Ayana, Lelisa Wogi, Jarosław Guziński

Faculty of Electrical and Control Engineering, Gdańsk University of Technology
11/12 Narutowicza str., 80-233 Gdańsk, Poland

e-mail: {✉ deevyas/marcin.morawiec/tadele.ayana/lelisa.wogi/jaroslaw.guzinski}@pg.edu.pl

(Received: 07.03.2024, revised: 23.08.2024)

Abstract: The use of the interior permanent magnet synchronous machine (IPMSM) drive has profoundly increased in a large number of applications due to numerous advantages. Owing to the disadvantages of mechanical sensors, sensorless control techniques are employed to enhance the performance of the IPMSM drive by removing the effect of noise and gain drift due to the sensor, increasing reliability, cost saving, and reducing overall size. This article presents the comparative analysis between the adaptive observer and non-adaptive extended electromotive force (EEMF) observer based on the active flux concept in a stationary reference frame (α–β). Moreover, the effect of slot harmonics and non-sinusoidal distribution of rotor flux is present in the three-phase IPMSM, this problem is considered as the control system disturbances in this article. Due to the non-sinusoidal distribution of flux and slot harmonics, the observer structure in the rotating reference frame (d–q) fails to estimate at the low-speed operation range. Comparative analysis between adaptive and non-adaptive observer structures is provided for a wide speed range. The effectiveness of the observer structures is examined using the classical field-oriented control scheme. In the end, simulation and experimental results are demonstrated to validate the performance of the sensorless control scheme using the adaptive and non-adaptive observer structures for the three-phase IPMSM drive setup.

Key words: field oriented control, interior permanent magnet synchronous machine, model-based method, sensorless control, speed observer

1. Introduction

The permanent magnet synchronous machine (PMSM) is widely used in industrial applications: transportation, machine tools, robotics, and home appliances because of its key features such as high torque density, rapid dynamic response, high reliability, and good power factor. When permanent magnets are placed on the surface of the rotor, it is called a surface-mounted permanent magnet synchronous machine (SPMSM). In contrast, permanent magnets are buried inside the rotor in the interior permanent magnet synchronous machine (IPMSM). This paper considers the IPMSM throughout the discussion on sensorless control based on adaptive and non-adaptive estimation of speed and position. Sensorless control, also known as a self-sensing unit, is primarily used to lessen the cost and size of the system while improving its reliability compared to mechanical sensors. Sensorless control has drawn significant attention from researchers across academia and industries, which has helped to develop new sensorless control methods for a wide speed range of the IPMSM drive [1–6].

Sensorless control techniques for the IPMSM drive can be classified based on the zero and low-speed range as well as the medium and high-speed range. For zero and low-speed range operation, saliency-based methods such as rotating signal injection, pulsating signal injection, and arbitrary injection can be used [1, 20, 26]. In saliency-based methods, inductances play an important role as inductances contain the information of rotor position, which is essential for sensorless control. For medium and high-speed applications, model-based methods that involve an extended EMF model or flux linkage model can be subcategorized into the open loop as well as close loop control methods [1, 20, 26]. Recently, sensorless control techniques based on artificial intelligence have also been introduced [5–7].

An internal model control observer using predictive current control was implemented, but inaccuracy in estimation was observed due to disturbances. However, this method works well considering the feasibility, robustness, and control point of view [8]. A sliding mode observer based on Lyapunov stability criteria for estimation of speed and position was proposed, but the impact of an observer during low or zero speed range was not covered [9]. A rotor flux-based observer was proposed in [10] to estimate speed and position. A parameter estimator and flux observer-based regression model was proposed by J. Choi *et al*. This observer has also faced the issue of inaccuracy during zero or low speed [11]. An adaptive full-order observer based on a cascade design approach for the IPMSM is proposed in [12]. This observer structure reduced the number of tuning gains, but the proposed control scheme stagnated during the standstill position and failed to deliver the desired results at the zero-low speed range. A third-order super-twisting observer, a non-linear extended state observer, and a novel frequency adaptive second-order disturbance observer were presented in [13–15], respectively. For medium and high speed, [13–15] works well but suffers during zero-low speed. Other observer structures are also popular, such as Model reference adaptive systems, adaptive filters, and extended state observers, which are close-loop observer techniques [1, 20, 26]. Different observer structures for the IPMSM are mentioned in [16–18]. It is also possible that the implementation of the observer technique is not straightforward in engineering practice due to the complex structure of the observer.

In this article, we propose an adaptive full-order observer and a non-adaptive EEMF observer structure based on an active flux concept to estimate speed and position. The IPMSM used for this reserach contains spatial harmonics and a non-sinusoidal distribution of EMF. Considering

the above problem, an observer structure based on the (d–q) reference frame is not preferable because the transformation of the estimated rotor position from the (d–q) reference frame will suffer from disturbances. Hence, the observer structure based on the (α–β) reference frame is more robust during the disturbances as it does not require transformation to estimate the rotor position. This article presents an observer structure based on an adaptive full-order observer and an EEMF observer using non-adaptive estimation based on the (α–β) reference frame. Conventional adaptive laws are used to estimate rotor speed in the adaptive observer, which decreases the order of the observer structure, and by integrating the rotor speed, the angular position is calculated. In EEMF, observer speed is calculated using a non-adaptive approach. In non-adaptive estimation, speed is calculated using the dependence of extended EMF and a permanent magnet flux component, and the angular position is computed using the EEMF components. The main contributions of this paper are:

1. Provide a robust observer structure in the (α–β) reference frame for all speed ranges, considering the problem of spatial harmonics and the non-sinusoidal distribution of EMF in the IPMSM motor. The control system in the article is also assumed not to compensate the slot harmonics.
2. Deliver a comparative analysis between adaptive and non-adaptive observer structures for a wide speed range.

The proposed concepts are verified by theoretical work, simulation, and experimental implementation. The experimental work is performed on a 3.5 kW IPMSM with slot harmonics.

2. Mathematical model of IPMSM

The mathematical model of the IPMSM considered in this paper is in the (α–β) reference frame [19–22] and can be represented using the differential equation as given below.

$$\frac{\mathrm{d}i_{s\alpha}}{\mathrm{d}\tau} = -\frac{1}{L_q}R_s i_{s\alpha} + \frac{1}{L_q}\omega\psi_{f\beta} + \frac{1}{L_q}u_{s\alpha}, \tag{1}$$

$$\frac{\mathrm{d}i_{s\beta}}{\mathrm{d}\tau} = -\frac{1}{L_q}R_s i_{s\beta} - \frac{1}{L_q}\omega\psi_{f\alpha} + \frac{1}{L_q}u_{s\beta}, \tag{2}$$

$$\frac{\mathrm{d}\omega_r}{\mathrm{d}\tau} = \frac{1}{J}(\psi_{f\alpha}i_{s\beta} - \psi_{f\beta}i_{s\alpha}) - \frac{1}{J}T_L, \tag{3}$$

$$\frac{\mathrm{d}\theta_r}{\mathrm{d}\tau} = \omega_r. \tag{4}$$

Similarly, by applying state space in the stationary reference frame dynamic model for EEMF in the IPMSM, it can be modeled as [19–22].

$$\frac{\mathrm{d}i_{s\alpha}}{\mathrm{d}\tau} = -\frac{1}{L_q}R_s i_{s\alpha} + \frac{1}{L_q}e_\beta + \frac{1}{L_q}u_{s\alpha}, \tag{5}$$

$$\frac{\mathrm{d}i_{s\beta}}{\mathrm{d}\tau} = -\frac{1}{L_q}R_s i_{s\beta} - \frac{1}{L_q}e_\alpha + \frac{1}{L_q}u_{s\beta}, \tag{6}$$

$$\frac{\mathrm{d}e_\alpha}{\mathrm{d}\tau} = \frac{\mathrm{d}\omega_r}{\mathrm{d}\tau}\psi_{f\alpha} - \omega_r e_\beta, \tag{7}$$

$$\frac{\mathrm{d}e_\beta}{\mathrm{d}\tau} = \frac{\mathrm{d}\omega_r}{\mathrm{d}\tau}\psi_{f\beta} + \omega_r e_\alpha. \tag{8}$$

In the mathematical model, stator resistance is defined as R_s; magnetic anisotropy can be ignored by considering the rotor pole salient IPMSM into a fictitious rotor non-salient pole IPMSM, which reduces the complexity in the estimation process of speed and position. The inductance of the rotor of the IPMSM can be considered as L_q. $u_{s\alpha,\beta}$, $i_{s\alpha,\beta}$ and $\psi_{f\alpha,\beta}$ are the vector components of supplied voltage and current to stator terminals, and flux components of a permanent magnet, respectively. J, T_L, and T_e are known as the machine's inertia, load torque, and electromagnetic torque. Angular speed is ω_r, and angular position is θ_r. In the extended model, EMF is introduced. $e_{\alpha,\beta}$ is the vector component of EMF. The EMF $\boldsymbol{e}$ vector contains the information of angular position, which will be useful in the EEMF model. It is considered that the parameters of the IPMSM machine are unchanging with time. It is assumed that the machine operates in the operation domain D where $\boldsymbol{i}_s^{\max}$, $\boldsymbol{e}^{\max}$, $\omega_r^{\max}$, $T_L^{\max}$ are considered as the maximum value of the stator current vector, EMF vector, rotor speed and load torque such that $|\boldsymbol{i}_s| \leq \boldsymbol{i}_s^{\max}$, $|\boldsymbol{e}| \leq \boldsymbol{e}^{\max}$, $|\omega_r| \leq \omega_r^{\max}$, $|T_L| \leq T_L^{\max}$. It is assumed that $T_L^{\max} = T_{en}$ and $\boldsymbol{i}_s^{\max} \approx 1$ p.u.

As discussed earlier, the IPMSM contains the non-sinusoidal distribution of EMF with the additional problem of spatial harmonics. This paper will consider the above problems as control system disturbances. In the IPMSM, the 18$^{\text{th}}$-order harmonic is dominant as can be seen in Fig. 1.

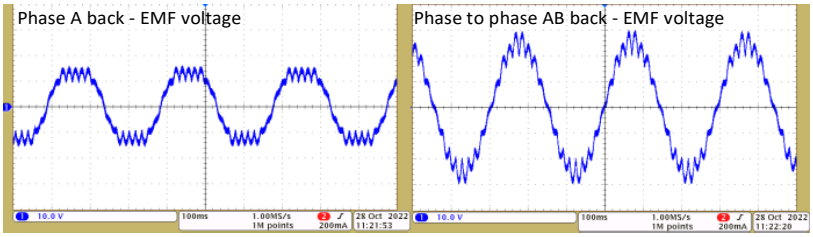

Fig. 1. Steady state of the machine, measured phase "A" EMF voltage and phase to phase A-B EMF voltage

The total number of slots is 36 in the IPMSM. In this article, 18$^{\text{th}}$-order harmonics are not compensated by implementing the extended control system. In the next section, an observer structure based on a mathematical model is prepared and discussed in detail.

3. Adaptive speed and position observer structure

Firstly, an observer structure based on adaptive mechanism will be discussed, and then an EEMF-based observer structure using non-adaptive estimation law will be covered. This paper implements an observer structure based on the (α–β) reference frame for an adaptive observer structure and EEMF-based non-adaptive structure. In the observer structure, "$\wedge$" is used to define the estimated state variable and "$\sim$" is defined as the error. considering the mathematical model, the observer structure has the following form:

$$\frac{\mathrm{d}\hat{i}_{s\alpha}}{\mathrm{d}\tau} = -\frac{1}{L_q}R_s\hat{i}_{s\alpha} + \frac{1}{L_q}\hat{\omega}_r\hat{\psi}_{f\beta} + \frac{1}{L_q}u_{s\alpha} + v_\alpha, \tag{9}$$

$$\frac{\mathrm{d}\hat{i}_{s\beta}}{\mathrm{d}\tau} = -\frac{1}{L_q}R_s\hat{i}_{s\beta} - \frac{1}{L_q}\hat{\omega}_r\hat{\psi}_{f\alpha} + \frac{1}{L_q}u_{s\beta} + v_\beta, \tag{10}$$

$$\frac{\mathrm{d}\hat{\theta}_r}{\mathrm{d}\tau} = \hat{\omega}_r. \tag{11}$$

v_α are v_β are the stabilizing functions added to the observer structure (9) and (10). The Lyapunov theorem finalizes the form of defined stabilizing functions. It can be seen in the observer model that $u_{s\alpha,\beta}$ represents the input state voltage vector components. $\hat{I}_{s\alpha,\beta}$ and $\hat{\psi}_{f\alpha,\beta}$ are defined as the vector components of the estimated currents, and the estimated components of permanent magnet flux in the (α–β) reference frame are calculated using the estimated angular position.

$$\hat{\psi}_{f\alpha} = \psi_f \cos\hat{\theta}_r, \tag{12}$$

$$\hat{\psi}_{f\beta} = \psi_f \sin\hat{\theta}_r. \tag{13}$$

Implementing stability analysis using the Lyapunov stability theorem can obtain the form of the stabilizing functions, v_α are v_β, to stabilize the observer structure. The error between the estimated state variable and measured value can be obtained from (14).

$$\begin{aligned}
\widetilde{i}_{s\alpha} &= \hat{i}_{s\alpha} - i_{s\alpha},\\
\widetilde{i}_{s\beta} &= \hat{i}_{s\beta} - i_{s\beta},\\
\widetilde{\omega}_r &= \hat{\omega}_r - \omega_r,\\
\widetilde{\theta}_r &= \hat{\theta}_r - \theta_r,
\end{aligned} \tag{14}$$

$$V = \frac{1}{2}\left(\widetilde{i}_{s\alpha}^2 + \widetilde{i}_{s\beta}^2\right). \tag{15}$$

Based on an estimation error, a positively determined function for the Lyapunov stability theorem is defined in (15), and then the function's derivative must be negatively determined, $\dot{V} \leq 0$. Substituting (14) to (15) gives the following equation:

$$\begin{aligned}
\dot{V} = \widetilde{i}_{sa}\left(-\frac{R}{L_q}\widetilde{i}_{s\alpha} + \frac{1}{L_q}\left(\hat{\omega}\left(\hat{\psi}_{f\beta} - \hat{\psi}_{f\beta}\right) - \widetilde{\omega}\left(\hat{\psi}_{f\beta} - \hat{\psi}_{f\beta}\right)\right) + v_\alpha\right) +\\
\widetilde{i}_{s\beta}\left(-\frac{R}{L_q}\widetilde{i}_{s\beta} - \frac{1}{L_q}\left(\hat{\omega}\left(\hat{\psi}_{f\alpha} - \hat{\psi}_{f\alpha}\right) - \widetilde{\omega}\left(\hat{\psi}_{f\alpha} - \hat{\psi}_{f\alpha}\right)\right) + v_\beta\right) \leq 0.
\end{aligned} \tag{16}$$

By introducing $c_\alpha > 0$ in the stabilizing functions v_α are v_β, the proposed observer structure becomes asymptotically stable, and the stabilizing functions have the following form:

$$v_\alpha = -c_\alpha\frac{R_s}{L_q}\widetilde{i}_{s\alpha}, \tag{17}$$

$$v_\beta = -c_\alpha\frac{R_s}{L_q}\widetilde{i}_{s\beta}. \tag{18}$$

To obtain an estimated speed, a positively defined Lyapunov function can be extended as

$$V_1 = \frac{1}{\gamma}\widetilde{\omega}_r^2. \tag{19}$$

The derivative of the positively defined function in (19) should be negatively determined as per the Lyapunov stability theorem as given in (20). With the help of adaptive mechanism, the value of the estimated speed can be calculated from (20) and expressed in (21) by assuming that $\dot{\widetilde{\omega}}_r \approx \dot{\hat{\omega}}_r$ and $\gamma > 0$.

$$\dot{V} = \widetilde{\omega}\left(\frac{1}{\gamma}\dot{\widetilde{\omega}} + \left(\hat{\psi}_{f\beta}\widetilde{i}_{s\alpha} - \hat{\psi}_{f\alpha}\widetilde{i}_{s\beta}\right)\right), \tag{20}$$

$$\dot{\widetilde{\omega}} = -\gamma\left(\hat{\psi}_{f\beta}\widetilde{i}_{s\alpha} - \hat{\psi}_{f\alpha}\widetilde{i}_{s\beta}\right). \tag{21}$$

4. Non-adaptive speed and position observer structure

The EEMF-based observer structure for the estimation of speed and position considering the non-adaptive is prepared based on the dynamic model, (5)–(8), and given as

$$\frac{\mathrm{d}\hat{i}_{s\alpha}}{\mathrm{d}\tau} = -\frac{1}{L_q}R_s\hat{i}_{s\alpha} + \frac{1}{L_q}\hat{e}_\beta + \frac{1}{L_q}u_{s\alpha} + v_\alpha, \tag{22}$$

$$\frac{\mathrm{d}\hat{i}_{s\beta}}{\mathrm{d}\tau} = -\frac{1}{L_q}R_s\hat{i}_{s\beta} - \frac{1}{L_q}\hat{e}_\alpha + \frac{1}{L_q}u_{s\beta} + v_\beta, \tag{23}$$

$$\frac{\mathrm{d}\hat{e}_\alpha}{\mathrm{d}\tau} = \frac{\mathrm{d}\hat{\omega}_r}{\mathrm{d}\tau}\hat{\psi}_{f\alpha} - \hat{\omega}_r\hat{e}_\beta + v_{e\alpha}, \tag{24}$$

$$\frac{\mathrm{d}\hat{e}_\beta}{\mathrm{d}\tau} = \frac{\mathrm{d}\hat{\omega}_r}{\mathrm{d}\tau}\hat{\psi}_{f\beta} + \hat{\omega}_r\hat{e}_\alpha + v_{e\beta}. \tag{25}$$

It can be seen that stabilizing functions v_α, v_β,$v_{e\alpha}$, and $v_{e\beta}$ are introduced in the observer structure (22)–(25). Without stabilizing functions, the observer can't converge to the real value of the machine, so this stabilizing function has significant importance. By considering $\mathrm{d}\hat{\omega}_r/\mathrm{d}\tau \approx \Delta\hat{\omega}_r/\Delta\tau$, the derivative of the speed given in (24) and (25) can be approximated, however this term does not affect the accuracy of the observer for the estimation of angular speed and position. The final form of the stabilizing function can be achieved using the Lyapunov stabilizing function. The error between estimation and measured value can be defined as (26). A positively determined Lyapunov function and its derivative, which is negatively determined $\dot{V} \leq 0$ are given (27) and (28).

$$\begin{aligned}
\widetilde{i}_{s\alpha,\beta} &= \hat{i}_{s\alpha,\beta} - i_{s\alpha,\beta},\\
\widetilde{e}_{\alpha,\beta} &= \hat{e}_{\alpha,\beta} - e_{\alpha,\beta},\\
\widetilde{\omega}_r &= \hat{\omega}_r - \omega_r,\\
\widetilde{\theta}_r &= \hat{\theta}_r - \theta_r,
\end{aligned} \tag{26}$$

$$V = \frac{1}{2}\left(\widetilde{i}_{s\alpha}^2 + \widetilde{i}_{s\beta}^2\right), \tag{27}$$

$$\dot{V} = \widetilde{i}_{sa}\left(-\frac{R}{L_q}\widetilde{i}_{s\alpha} + \frac{1}{L_q}\widetilde{e}_\beta + v_\alpha\right) + \widetilde{i}_{s\beta}\left(-\frac{R}{L_q}\widetilde{i}_{s\beta} - \frac{1}{L_q}\widetilde{e}_\alpha + v_\beta\right). \tag{28}$$

The proposed observer structure is asymptotic stable if v_α, v_β, $v_{e\alpha}$, and $v_{e\beta}$ have the following form given in (29) to (32). Gains c_α, $c_{e\alpha}$, and $c_{e\beta}$ are > 0.

$$v_\alpha = -c_\alpha \frac{R_s}{L_q} \widetilde{i}_{s\alpha}, \tag{29}$$

$$v_\beta = -c_\alpha \frac{R_s}{L_q} \widetilde{i}_{s\beta}, \tag{30}$$

$$v_{e\alpha} = c_{e\alpha} \frac{1}{L_q} \widetilde{i}_{s\beta}, \tag{31}$$

$$v_{e\beta} = -c_{e\beta} \frac{1}{L_q} \widetilde{i}_{s\alpha}. \tag{32}$$

The estimation of angular speed using the non-adaptive approach defined in (33) can be computed using dependencies of EEMF and components of permanent magnet flux [23]. Similarly, the angular position can be estimated using the angle observer between the EEMF defined in (34). Flux components tend to have real value in finite time as well and the speed will also reach their real value exponentially.

$$\hat{\omega}_r = \frac{\hat{e}_\alpha \hat{\psi}_{f\alpha} + \hat{e}_\beta \hat{\psi}_{f\beta}}{\hat{\psi}_{f\alpha}^2 + \hat{\psi}_{f\beta}^2}, \tag{33}$$

$$\hat{\theta}_r = a \tan(\hat{e}_\beta \hat{e}_\alpha). \tag{34}$$

5. Sensorless control scheme of IPMSM drive

The classical field-oriented control (FOC) is implemented as shown in Fig. 2. In this article, the classical FOC scheme considering $i_{sd}^* = 0$ is implemented. The classical control scheme transforms stator phase currents from (abc) to the (α–β) reference frame using the Clarke transformation for observer structure implementation. The observer structure estimates the state variables such as speed, position, and currents in the (α–β) reference frame. The estimated currents in the (α–β) reference frame are the transformed (d–q) reference frame using the Park transformation for control

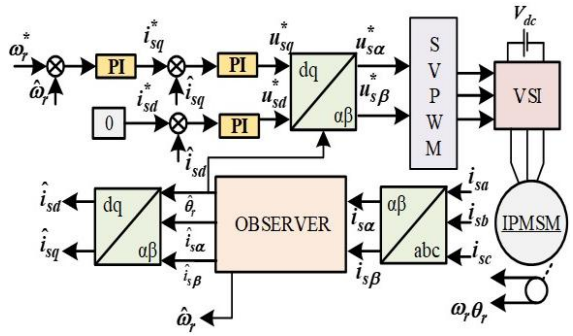

Fig. 2. Block diagram of sensorless field-oriented control scheme

structure implementation. Three controllers are used in the control structure: a speed controller and two for the turrent controller. The speed controller compares the reference value of speed (ω_r^*) and estimated speed ($\hat{\omega}_r$), and generates the error signal. Based on the error signal the reference value of torque is generated, represented by i_{sq}^*. The current controller, which compares the reference currents with estimated currents and is based on the error signal, as well as the reference voltage command is provided to the inverter. The observer gains for adaptive structures for simulation and experimental purposes are $c_\alpha = 0.7$ and $c_\alpha = 2.5$, respectively. For the non-adaptive structure, $c_\alpha = 3.5$, $c_{e\alpha} = 0.9$ and $c_{e\beta} = 0.9$ are used for simulation and experimental work.

In Figure 3, the simulation result of the three-phase IPMSM drive starting up to nominal speed is shown.

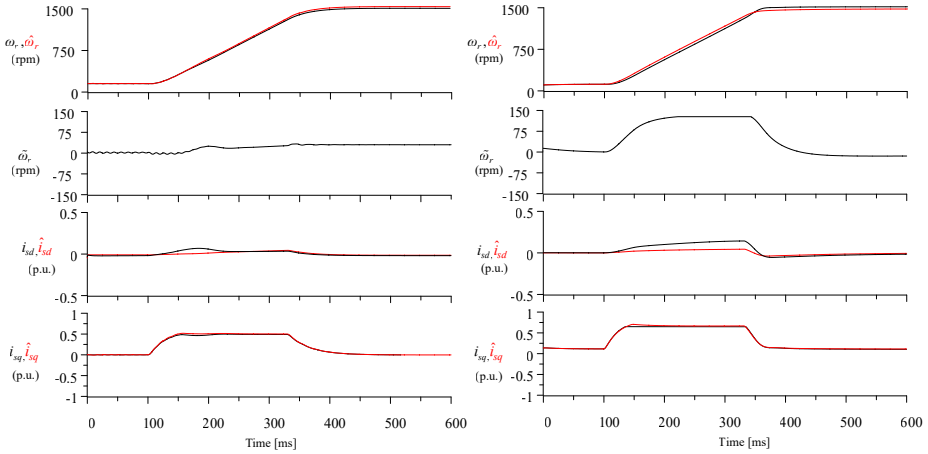

Fig. 3. Simulation results of IPMSM drive starting up to nominal speed: (a) adaptive observer structure; (b) non-adaptive observer structure

The performance of the sensorless control system using the adaptive observer structure and non-adaptive observer structure is shown in Fig. 3(a) and Fig. 3(b), respectively. Measured speed (ω_r), estimated speed ($\hat{\omega}_r$), speed estimation error ($\widetilde{\omega}_r$), measured flux controlling (i_{sd}) and torque controlling (i_{sq}) components, and estimated flux controlling ($\hat{i}_{sd}$) and torque controlling components ($\hat{i}_{sq}$) in dq coordinate systems are shown in Fig. 3(a) and Fig. 3(b). It can be observed that the speed estimation error was high around 140 rpm in Fig. 3(b), while the speed error was less than 35 rpm in Fig. 3(a) during the dynamic state.

The reversal of the three-phase IPMSM drive from 1500 rpm to –1500 rpm using adaptive and non-adaptive observer structures is depicted in Fig. 4(a) and Fig. 4(b), respectively. In Fig. 4(a), the IPMSM drive can cross zero speed and reaches –1500 rpm using an adaptive observer structure. In Fig. 4(b), when the IPMSM drive reverses from 1500 rpm, it struggles at zero speed. Near zero speed, the value of back EMF is very small, and the estimated speed depends on the EMF; hence, the IPMSM drive struggles at zero speed. Parameters such as measured speed (ω_r), estimated speed ($\hat{\omega}_r$), speed estimation error ($\widetilde{\omega}_r$), measured angular position (θ_r), estimated angular position ($\hat{\theta}_r$), position estimation error ($\widetilde{\theta}_r$), measured q-axis current (i_{sq}) and estimated q-axis components ($\hat{i}_{sq}$) are shown in Fig. 4.

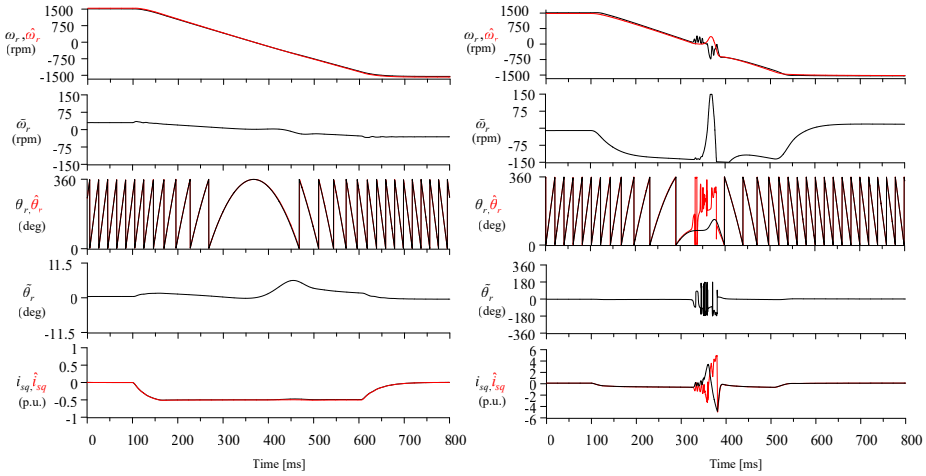

(a) (b)

Fig. 4. Simulation results of IPMSM drive reversing up from 1500 rpm to –1500 rpm: (a) adaptive observer structure; (b) non-adaptive observer structure

In Fig. 5 and Fig. 6, sensorless control scheme using adaptive and non-adaptive observer structures was tested against load injection and load removal, respectively. In Fig. 5, the speed of the three-phase IPMSM was set at 750 rpm, and after 0.1 s, the load was applied up to 0.5 p.u. as shown. Parameters of the sensorless control system using the adaptive observer structure and non-adaptive observer structure are shown in Fig. 5(a) and Fig. 5(b), respectively. In Fig. 6. the IPMSM drive was rotating at 750 rpm, and the load was disconnected after 0.1 s, as shown. Speed

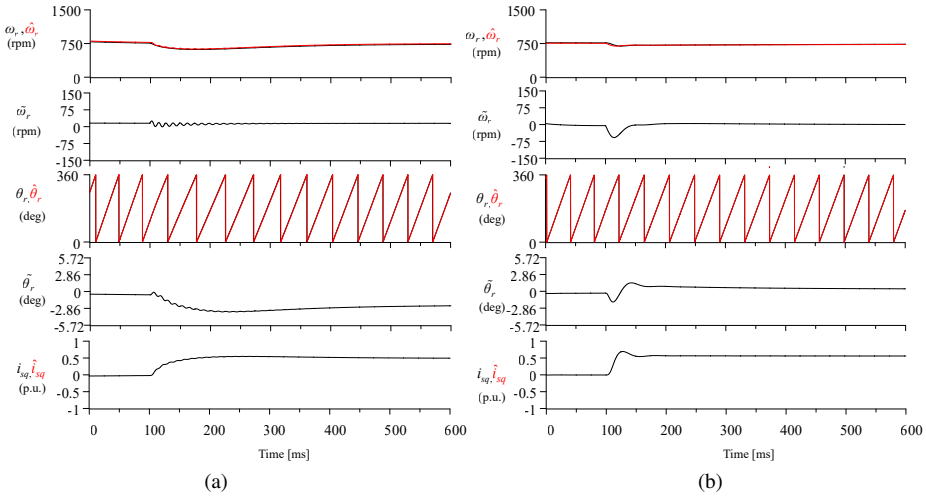

(a) (b)

Fig. 5. Simulation results of IPMSM drive, when speed is set at 750 rpm and load is injected up to 0.5 p.u.: (a) adaptive observer structure; (b) non-adaptive observer structure

estimation error and position estimation error in the adaptive observer structure and non-adaptive observer structure were also in the acceptable range, as shown in Fig. 5 and Fig. 6. Both the observer structures work well in the case of load injection and load removal.

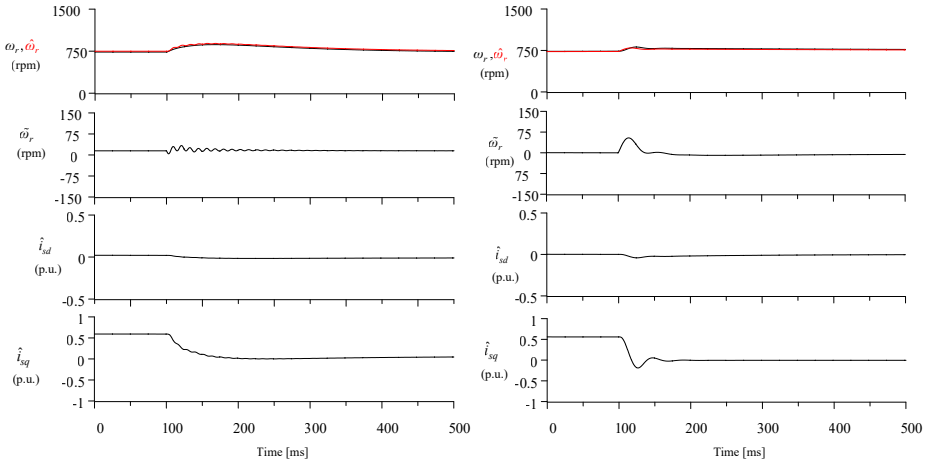

Fig. 6. Simulation results of IPMSM drive, when speed is set 750 rpm and load is disconnected: (a) adaptive observer structure; (b) non-adaptive observer structure

6. Experimental results and discussion

The performance of the sensorless control system using the adaptive observer structure and non-adaptive observer structure is evaluated in real-time operating conditions using the set of laboratory equipment. The experimental test was carried out on a 3.5 kW IPMSM drive system. As shown in Fig. 1, the non-sinusoidal distribution of back-EMF is present in the IPMSM. A voltage source converter supplies the drive system. All the nominal parameters of the IPMSM drive are given in Table 1. The control system was interfaced with a DSP *Sharc* ADSP21363 floating-point signal processor and Altera Cyclone 2 FPGA with a sampling time of 150 μs (6.6 kHz). The switching frequency of the transistor was 3.3 kHz.

The control system structure can be seen in Fig. 2. To measure the current in natural reference frame, an LA 25-NP transducer was used. To implement the observer structure in the stationary reference frame, the measured current was transformed to the (α–β) coordinate system using the Clarke transformation. The computation time of the control system is 49 μs without applying code optimization. The incremental encoder of 11 bits was used to measure the speed of the three-phase IPMSM drive. The only purpose of using the encoder was to confirm the estimation accuracy of the observer structures. Tuning gains of the PI controllers for field-oriented control are given in Table 2.

The observer structure is based on a sinusoidal machine model. Considering Fig. 1, slot harmonics are treated as disturbances for observer systems that have bounded values and frequencies. These disturbances significantly affect the low-speed operation of the IPMSM drive, as shown

Table 1. Parameters of the IPMSM

Parameter name	**Symbol**	**Value**	**Unit**
Stator resistance	R_{sN}	0.035	p.u.
d-axis inductances	L_{dN}	0.28	p.u.
q-axis inductances	L_{qN}	0.82	p.u.
Permanent magnet flux linkage	ψ_f	0.89	p.u.
Nominal value of electromagnetic torque	TeN	0.81	p.u.
Nominal power	Pn	3.5	kW
Nominal stator current (y)	In	7.5	A
Nominal stator voltage (y)	Un	285	V
Nominal rotor speed	n	1500	rpm
Nominal frequency	F	50	Hz
Reference voltage	$Ub = Un$	285	V
Reference current	$I_b = \sqrt{3}I_n$	12.97	A

Table 2. Tuning gains of the field-oriented control system

Parameter name	**Symbol**	**Gains**
Proportional gain for speed controller	$K_{p\omega}$	5
Integral gain for speed controller	$K_{i\omega}$	0.02
Proportional gain for d-axis current controller	K_{pid}	3.5
Integral gain for d-axis current controller	K_{iid}	0.1
Proportional gain for q-axis current controller	K_{piq}	2
Integral gain for $q_{(2)}$-axis current controller	K_{iiq}	0.1

in Fig 7. In Fig. 7(a), the IPMSM drive successfully reverses from –150 rpm to 150 rpm using the estimated rotor position, but in Fig. 7(b), the IPMSM drive struggles during reversing at zero speed. However, due to disturbances, oscillations are present at the estimated speed. Extending the control system to the damping structure presented in [24, 25] can compensate for this oscillation. However, this article only focuses on speed observer structure; the problem of non-sinusoidal EMF is treated as a disturbance. A low-pass filter (LPF) can be implemented to minimize the disturbances.

In Fig. 8, the IPMSM is starting up from 150 rpm to 1500 rpm. It can be seen that the estimated variables using both types of observer structures work at medium and high speed but struggle at low speed. Speed error was less than 50 rpm for both observer structures. When speed changes from 150 rpm to 1500 rpm, the estimated q-axis current, which is known as torque representing a component, increases from 0 and reaches 0.5 p.u. and during a steady state when speed reaches

1500 rpm again, it becomes zero as no-load is connected. Parameters of the adaptive observer structure and non-adaptive observer structure such as measured speed (ω_r), estimated speed ($\hat{\omega}_r$), speed estimation error ($\widetilde{\omega}_r$), angular position error (θ_r), estimated angular position ($\hat{\theta}_r$), and estimated q-axis components ($\hat{i}_{sq}$) are shown in Fig. 8.

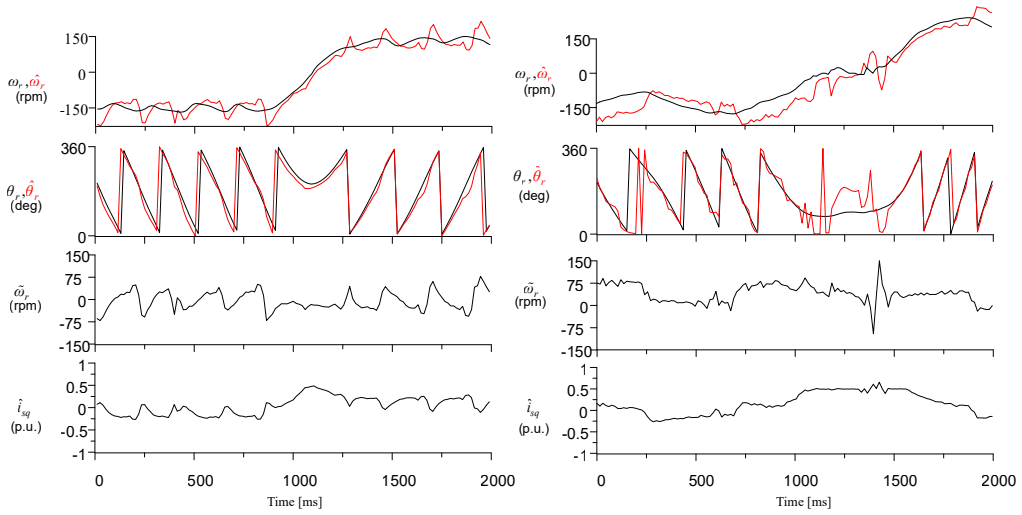

Fig. 7. Experimental results of IPMSM drive reversing up from –150 rpm to 150 rpm: (a) adaptive observer structure; (b) non-adaptive observer structure

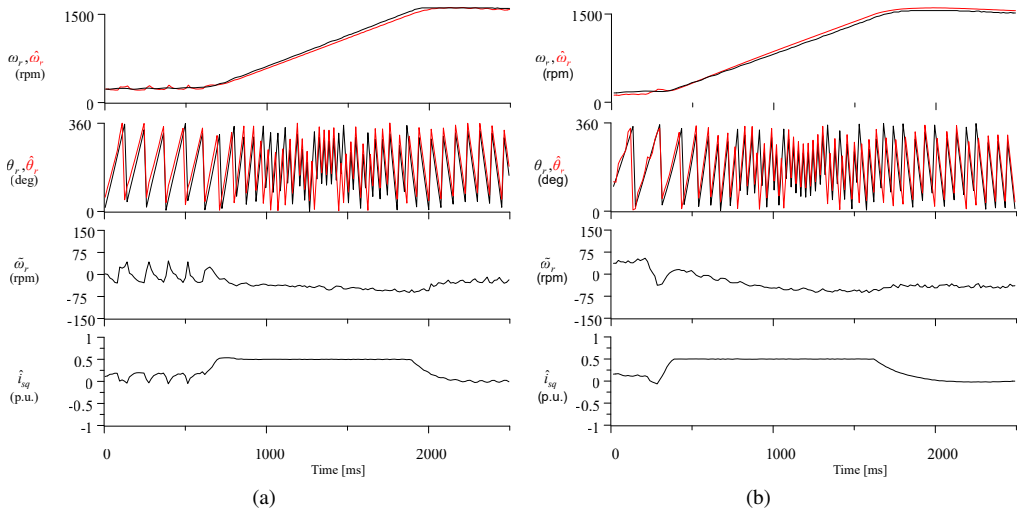

Fig. 8. Experimental results of IPMSM drive starting up to 1500 rpm: (a) adaptive observer structure; (b) non-adaptive observer structure

Figure 9 presents the workings of the adaptive observer structure during IPMSM reversal from 1500 rpm to –1500 rpm. The result shows that the estimated speed crosses the zero speed range without any problem. The error between the estimated angular position and measured position ($\widetilde{\theta_r}$) is also shown. The estimated stator current components in the d–q coordinate system are also shown as ($\hat{i}_{sd}$) and ($\hat{i}_{sq}$).

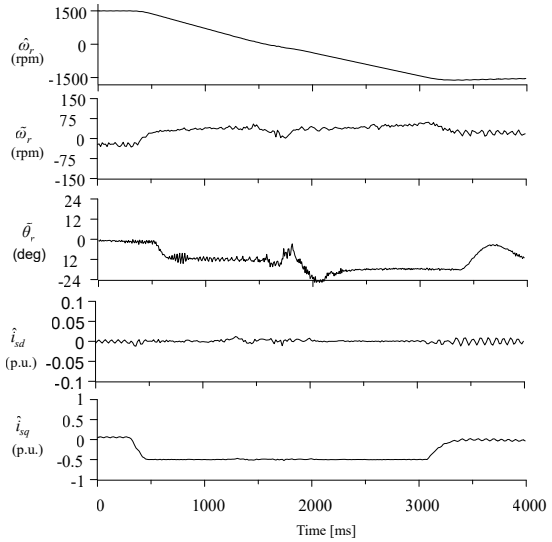

Fig. 9. Experimental results of IPMSM drive reversing from 1500 rpm to –1500 rpm using adaptive observer structure

Figure 10(a) and Fig. 10(b) show non-adaptive estimation using an EEMF-based observer structure for the IPMSM drive reversing from 1500 rpm to –1500 rpm and –1500 rpm to 1500 rpm, respectively. During zero crossing, non-adaptive speed estimation struggles in both cases; however, it reaches the maximum value again, but at zero speed, it does not provide a satisfactory results. Speed error and position error are high compared to the adaptive structure. In Fig. 10, the EEMF observer structure struggles at zero speed because at zero speed, the value of back EMF is very small, which is not enough to estimate speed; hence, the observer structure fails to estimate during extremely low speed of the IPMSM.

In Fig. 11, the rotor speed was set at 750 rpm, and load torque ≈ 0.75 p.u. was injected at 0.1 s. In Fig. 11(a), the performance of the adaptive observer structure can be visualized. Speed estimation error was less than 30 rpm, electromagnetic torque increases from zero and reaches ≈ 0.75 p.u. Figure 11(b) shows the non-adaptive observer structure's performance in the load injection case. When the load was injected after 0.1 s, the error in speed estimation was increased up to 140 rpm. It can be seen that the adaptive observer structure is more reliable and provides satisfactory results than the non-adaptive observer structure. A comparative analysis between the two observer structures is provided in Table 3 for a wide speed range.

The effect of the non-sinusoidal distribution of EMF is visible at the low-speed operation range for adaptive and non-adaptive observer structures. The adaptive observer structure can cross at zero speed, while the performance of the non-adaptive EEMF observer is acceptable for medium

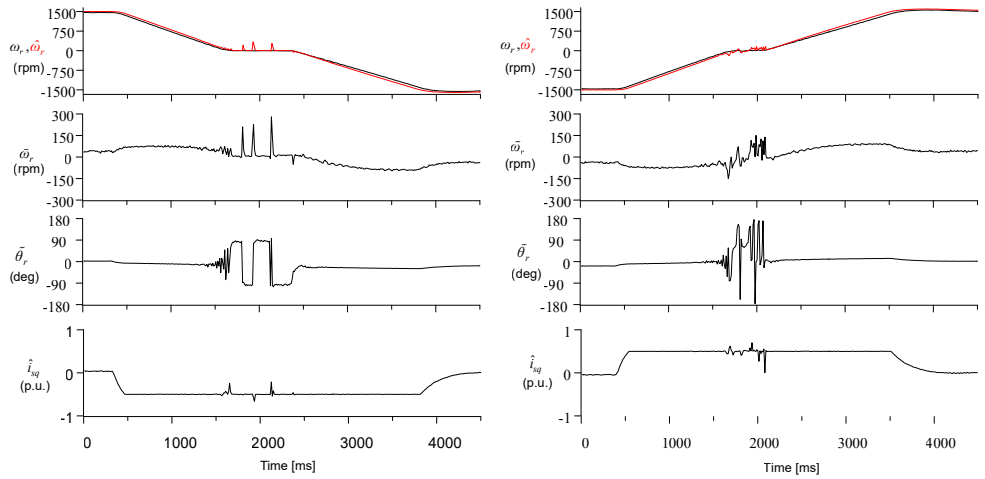

Fig. 10. Experimental results of IPMSM drive reversing from 1500 rpm to –1500 rpm using non-adaptive observer structure

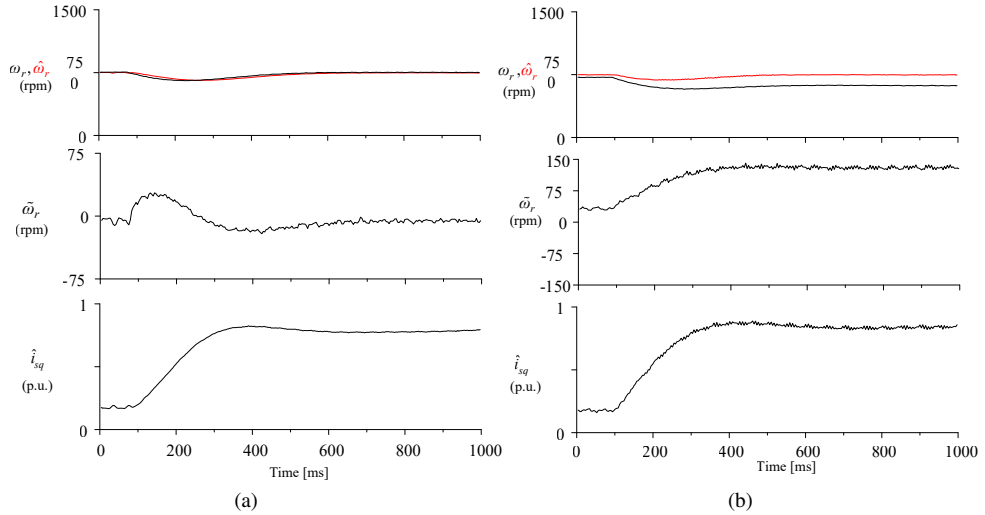

Fig. 11. Experimental results of IPMSM drive, when speed is set at 750 rpm and load is injected up to 0.5 p.u.: (a) adaptive observer structure: (b) non-adaptive observer structure

and high-speed operations. However, at zero-speed or very low speed, the amplitude of back EMF is very small. Hence, the signal used for estimation is very weak and can be easily contaminated by the measurement noises or nonlinear effect of the PWM inverter. In addition, parameters such as resistance and inductance have a very significant impact at low speed where the voltage drop is large compared to EMF voltage. Moreover, the signal can be lost in heavy-load conditions due to magnetic saturation; this problem is still open for research [26].

Table 3. Comparison of observer structures at a wide speed range

Name	Zero speed	Low speed	Medium speed	High speed
Adaptive observer structure	Stable	Stable	Stable	Stable
Non-adaptive EEMF based	Unstable	Unstable	Stable	Stable

Fig. 12. Photo of experimental stand with the IPMSM clutched to DC machine

7. Conclusion

This article presented rotor speed and position estimation using adaptive observer and non-adaptive observer structures based on an EEMF model for the sensorless IPMSM drive in the (α–β) reference frame. Adaptive laws are implemented to estimate rotor speed in the case of the adaptive observer structure, and in the non-adaptive EEMF observer structure, the rotor speed is calculated using dependences EMF and flux components. The final form of the stabilizing function can be derived with the help of Lyapunov's stability theorem. Considering the disturbances such as the non-sinusoidal distribution of EMF and slot harmonics, observer structures work well, specifically adaptive observer structures. The non-adaptive EEMF-based observer structure struggles during zero crossing. Both the observer structures presented in the articles are tested in simulation as well as on an experimental stand, and confirm the behavior of the observer structure at a wide speed range. Moreover, the proposed work can be extended to compensate for the slot harmonics and non-sinusoidal distribution of EMF.

References

[1] Wang G., Valla M., Solsona J., *Position sensorless permanent magnet synchronous machine drives – A review*, IEEE Transactions on Industrial Electronics, vol. 67, no. 7, pp. 5830–5842 (2020), DOI: 10.1109/TIE.2019.2955409.

[2] Ogbuka C., Nwosu C., Agu M., *Dynamic and steady state performance comparison of line-start permanent magnet synchronous motors with interior and surface rotor magnets*, Archives of Electrical Engineering, vol. 65, no. 1, pp. 105–116 (2016), DOI: 10.1515/AEE-2016-0008.

[3] Mlot A., Kowol M., Kolodziej J., Lechowicz A., Skrobotowicz P., *Analysis of IPM motor parameters in an 80-kW traction motor*, Archives of Electrical Engineering, vol. 69, no. 2, pp. 467–481 (2020), DOI: 10.24425/aee.2020.133038.

[4] Ryndzionek R., Blecharz K., Kutt F., Michna M., Kostro G., *Fault-Tolerant Performance of the Novel Five-Phase Doubly-Fed Induction Generator*, IEEE Access, vol. 10, pp. 59350–59358 (2022), DOI: 10.1109/ACCESS.2022.3179815.

[5] Młot A., Korkosz M., Lechowicz A., Podhajecki J., Rawicki S., *Electromagnetic analysis, efficiency map and thermal analysis of an 80-kW IPM motor with distributed and concentrated winding for electric vehicle applications*, Archives of Electrical Engineering, vol. 71, no. 4, pp. 981–1002 (2022), DOI: 10.24425/aee.2022.142120.

[6] Brock S., Pajchrowski T., *Sensorless and energy-efficient PMSM drive for fan application*, in Archives of Electrical Engineering, vol. 62, no. 2, pp. 217–225 (2013), DOI: 10.2478/aee-2013-0017.

[7] Li Y., Hu H., Shi P., *A Review of Position Sensorless Compound Control for PMSM Drives*, World Electric Vehicle Journal, vol. 14, no. 2, MDPI (2023), DOI: 10.3390/wevj14020034.

[8] Tang M., Wang C., Luo Y., *Predictive current control for permanent magnet synchronous motor based on internal model control observer*, Archives of Electrical Engineering, vol. 71, no. 2, pp. 343–362 (2022), DOI: 10.24425/aee.2022.140715.

[9] Navaneethan S., Kanthalakshmi S., Aandrew Baggio S., *Lyapunov stability based sliding mode observer for sensorless control of permanent magnet synchronous motor*, Bulletin of the Polish Academy of Sciences: Technical Sciences, vol. 70, no. 2 (2022), DOI: 10.24425/bpasts.2022.140353.

[10] Morawiec M., Lewicki A., Odeh C., *Rotor-Flux Vector based Observer of Interior Permanent Synchronous Machine*, IEEE Transactions on Industrial Electronics (2023), DOI: 10.1109/TIE.2023.3250851.

[11] Choi J., Nam K., Bobtsov A., Ortega R., *Sensorless Control of IPMSM Based on Regression Model*, IEEE Trans. on Power Electron., vol. 34, no. 9, pp. 9191–9201 (2019), DOI: 10.1109/TPEL.2018.2883303.

[12] Volpato Filho C., Vieira P., *Adaptive Full-Order Observer Analysis and Design for Sensorless Interior Permanent Magnet Synchronous Motors Drives*, IEEE Transactions on Industrial Electronics, vol. 68, no. 8, pp. 6527–6536 (2021), DOI: 10.1109/TIE.2020.3007101.

[13] Zhang T., Xu Z., Li J., Zhang H., Gerada C., *A third-order super-twisting extended state observer for dynamic performance enhancement of sensorless IPMSM drives*, IEEE Transactions on Industrial Electronics, vol. 67, no. 7, pp. 5948–5958 (2020), DOI: 10.1109/TIE.2019.2959498.

[14] Xu Z., Zhang T., Bao Y., Zhang H., Gerada C., *A nonlinear extended state observer for rotor position and speed estimation for sensorless IPMSM Drives*, IEEE Trans. on Power Electron., vol. 35, no. 1, pp. 733–743 (2020), DOI: 10.1109/TPEL.2019.2914119.

[15] Woldegiorgis A., Ge X., Wang H., Hassan M., *A New Frequency Adaptive Second-Order Disturbance Observer for Sensorless Vector Control of Interior Permanent Magnet Synchronous Motor*, IEEE Transactions on Industrial Electronics, vol. 68, no. 12, pp. 11847–11857 (2021), DOI: 10.1109/TIE.2020.3047065.

[16] Woldegiorgis A., Ge X., Li S., Hassan M., *Extended Sliding Mode Disturbance Observer-Based Sensorless Control of IPMSM for Medium and High-Speed Range Considering Railway Application*, IEEE Access, vol. 7, pp. 175302–175312 (2019), DOI: 10.1109/ACCESS.2019.2957274.

[17] Xiao D., Nalakath S., Sun Y., Wiseman J., Emadi A., *Complex-coefficient adaptive disturbance observer for position estimation of IPMSMs with robustness to DC Errors*, IEEE Transactions on Industrial Electronics, vol. 67, no. 7, pp. 5924–5935 (2020), DOI: 10.1109/TIE.2019.2941157.

[18] Zhang Y., Yin Z., Bai C., Wang G., Liu J., *A Rotor Position and Speed Estimation Method Using an Improved Linear Extended State Observer for IPMSM Sensorless Drives*, IEEE Trans. On Power Electron., vol. 36, no. 12, pp. 14062−14073 (2021), DOI: 10.1109/TPEL.2021.3085126.

[19] Krishnan R., *Permanent magnet synchronous and brushless DC motor drives*, CRC Press/Taylor & Francis (2010), DOI: 10.1201/9781420014235.

[20] Wang G., Zhang G., Xu D., *Position Sensorless Control Techniques for Permanent Magnet Synchronous Machine Drives*, Springer (2020), DOI: 10.1007/978-981-15-0050-3.

[21] Boldea I., Paicu M., Andreescu G., *Active flux concept for motion-sensorless unified AC drives*, IEEE Trans Power Electron, vol. 23, no. 5, pp. 2612–2618 (2008), DOI: 10.1109/TPEL.2008.2002394.

[22] Boldea I., Paicu M., Andreescu G., Blaabjerg F., *'Active Flux' DTFC-SVM sensorless control of IPMSM*, IEEE Transactions on Energy Conversion, vol. 24, no. 2, pp. 314–322 (2009), DOI: 10.1109/TEC.2009.2016137.

[23] Morawiec M., Blecharz K., *Non-adaptive Speed and Position Estimation of Doubly-Fed Induction Generator in Grid-Connected Operations*, IEEE Transactions on Industrial Electronics (2023), DOI: 10.1109/TIE.2023.3279548.

[24] Kim J., Doki S., Ishida M., *Improvement of IPMSM sensorless control performance by suppression of harmonics on the vector control using Fourier transform and repetitive control*, IEEE 2002 28th Annual Conference of the Industrial Electronics Society, IECON 02, Seville, Spain, vol. 1, pp. 597–602 (2002), DOI: 10.1109/IECON.2002.1187575.

[25] Mao Y., Yang J., Yin D., Chen Y., *Sensorless IPMSM control based on an extended nonlinear observer with rotational inertia adjustment and equivalent flux error compensation*, Journal of Power Electronics, vol. 16, no. 6, pp. 2150–2161 (2016), DOI: 10.6113/JPE.2016.16.6.2150.

[26] Sul S., Kwon Y., Lee Y., *Sensorless Control of IPMSM for Last 10 Years and Next 5 Years*, CES Transactions on Electrical Machines and Systems, vol. 1, no. 2, pp. 91–99 (2017), DOI: 10.23919/TEMS.2017.7961290.